

RESEARCH ARTICLE | FEBRUARY 06 2024

## Competition between the source and loss processes of radiation belt source, seed, and relativistic electrons induced by a magnetic cloud event

Zhengyang Zou (邹正洋)  ; Pingbing Zuo (左平兵)   ; Binbin Ni (倪彬彬)  ; Jiayun Wei (魏佳筠)  ; Wentao Zhou (周文涛) ; Hanyu Huang (黄瀚宇)  ; Yanqiong Xie (解妍琼)



*Physics of Fluids* 36, 026603 (2024)

<https://doi.org/10.1063/5.0186605>



CrossMark

07 February 2024 05:48:15



## Physics of Fluids

Special Topic:  
Selected Papers from the 2023 Non-Newtonian Fluid Mechanics Symposium in China

**Submit Today**



# Competition between the source and loss processes of radiation belt source, seed, and relativistic electrons induced by a magnetic cloud event

Cite as: Phys. Fluids **36**, 026603 (2024); doi: 10.1063/5.0186605

Submitted: 7 November 2023 · Accepted: 9 January 2024 ·

Published Online: 6 February 2024



View Online



Export Citation



CrossMark

Zhengyang Zou (邹正洋),<sup>1,2</sup> Pingbing Zuo (左平兵),<sup>2,3,a</sup> Binbin Ni (倪彬彬),<sup>4</sup> Jiayun Wei (魏佳筠),<sup>2,3</sup> Wentao Zhou (周文涛),<sup>1</sup> Hanyu Huang (黄瀚宇),<sup>1</sup> and Yanqiong Xie (解妍琼)<sup>5</sup>

## AFFILIATIONS

<sup>1</sup>State Key Laboratory of Lunar and Planetary Sciences, Macau University of Science and Technology, Macau, China

<sup>2</sup>Shenzhen Key Laboratory of Numerical Prediction for Space Storm, Institute of Space Science and Applied Technology, Harbin Institute of Technology, Shenzhen, China

<sup>3</sup>Key Laboratory of Solar Activity and Space Weather, National Space Science Center, Chinese Academy of Sciences, Beijing, China

<sup>4</sup>Department of Space Physics, School of Electronic Information, Wuhan University, Wuhan, Hubei, China

<sup>5</sup>College of Advanced Interdisciplinary Studies, National University of Defense Technology, Changsha, Hunan, China

<sup>a</sup>Author to whom correspondence should be addressed: pbzuo@hit.edu.cn

## ABSTRACT

The radiation belt energetic electrons that are trapped by the geomagnetic field are one kind of space plasma and magnetic fluid. We quantitatively study the competition process between source and loss processes of radiation belt “source” (a few to tens of keV), “seed” (hundreds of keV), and “relativistic” ( $>1$  MeV) electrons when a typical magnetic cloud (MC) event impinged on the magnetosphere on 19–20 July 2016. A very weak geomagnetic storm with  $\text{SymH}_{\min} = -32$  nT was driven by this magnetic cloud event. With the MC-driven shock arrival, the relativistic electrons experienced a “one-kick” energization at lower L-shells while having a moderate dropout at higher L-shells. The dropout became pronounced during the weak storm main phase. However, the seed electrons had a slight depletion after the shock and recovered to the pre-event level in the main phase, while the source electrons continued increasing during the entire event. Further analysis demonstrates that the loss processes (magnetopause shadowing and ultralow-frequency waves-driven outward transport) were competing with the source processes (shock-induced energization, substorm ejections, and wave–particle interactions), which are strongly sensitive to electron energy and L-shells. It is found that  $L^* \approx 4$  and  $\mu = 10^2\text{--}10^{2.5}$  MeV/G could be typical values at which the source and loss processes arrived at dynamic equilibrium. Our study first provides the “balance lines” in both energy channels and  $L^*$  of the radiation belt source, seed, and relativistic electrons in response to magnetic cloud events. The quantitative results could be a key factor when investigating MC–magnetosphere coupling.

Published under an exclusive license by AIP Publishing. <https://doi.org/10.1063/5.0186605>

## I. INTRODUCTION

The populations in the Earth’s radiation belt naturally evolve in a dynamic equilibrium that is influenced by kinds of solar winds.<sup>1–8</sup> During both quiescent and disturbed conditions, the coupling between the Earth’s magnetosphere and the solar wind can drive a large-scale sudden source or loss of radiation belt electrons, which can drastically redistribute the profile of the radiation belts for a few hours.<sup>1,9–16</sup>

The sudden loss of radiation belt electrons, also called “dropout,” is widely regarded as induced by (i) magnetopause shadowing as well as outward transport with electron losses to the interplanetary

space<sup>5,17–23</sup> and (ii) plasma waves (e.g., electromagnetic ion cyclotron waves, EMIC) leaded wave–particle interactions with electrons precipitated into the atmosphere.<sup>4,5,21,24–30</sup> Recent studies have demonstrated that dropout events always occur with persistent high solar wind dynamic pressure via compression of the magnetopause, a sharp negative phase space density (PSD) gradient, or ultralow-frequency (ULF) wave-caused outward diffusion.<sup>2,9,20,22,23,31–34</sup>

The sudden increase in the radiation belt electrons is distinctly energy dependent. Following the interplanetary (IP) shock, relativistic electron fluxes were observed with periodical enhancements.

Possible explanations include (i) one-kick energizations by azimuthal electric field impulses and subsequent drift echoes<sup>35,36</sup> and (ii) modulations by ultralow-frequency wave (ULF)-induced energizations.<sup>33,37–40</sup> For electrons at lower energies (e.g., source electrons at a few to tens of keV and seed electrons at hundreds of keV), the injections and convections during the substorms can also be regarded as one important source process.<sup>41</sup> In addition to directly changing the profile of the radiation belt, wave-particle intersections also play an important role in accelerating electrons. It has been suggested that the instability of substorm injected populations can potentially excite a variety of plasma waves, such as the whistler-mode chorus, which is capable of accelerating energetic electrons in the heart of the radiation belt within a few hours.<sup>1,26,27,42–45</sup>

Since both direct source or loss by magnetic field torturing and wave-induced modulations are all dominated by the interactions between the solar wind and the magnetosphere, the sudden flux enhancement of radiation belt electrons at different energies is sensitive to solar wind disturbances. Foster *et al.*<sup>35</sup> compared the PSD of relativistic electrons before and after the IP shock and provided evidence that shock-induced prompt acceleration and magnetopause shadowing can redistribute the profile of radiation belt relativistic electrons. In this investigation, we not only focus on the variability of relativistic electrons ( $>1$  MeV) but also study in detail the electron PSD change in a more comprehensive range of electron energies (from  $\sim 50$  eV to  $<1$  MeV) during a special magnetic cloud event. By tracing and comparing their evolution at different stages of the MC-magnetosphere coupling, we underline the importance and complexity of the competition processes and try to provide quantitatively the balance lines at which the source and loss processes arrived at dynamic equilibrium.

## II. DATA AND METHODOLOGY

In this study, the magnetic field and plasma data are derived from the magnetic and field investigation (MFI) and solar wind experiment (SWE) instruments<sup>46,47</sup> onboard the WIND spacecraft. The 1-min-average solar wind plasma and magnetic field data, as well as geomagnetic indices including Dst and AE, are downloaded from the NASA/OMNI database. The electron pitch angle resolved fluxes are obtained from the Relativistic Electron Proton Telescope (REPT) and the Magnetic Electron Ion Spectrometer (MagEIS) instruments onboard Van Allen Probes.<sup>48,49</sup> Here, we convert the electron fluxes to phase space density (PSD) under the TS04 geomagnetic field model<sup>50</sup> by applying the method used in previous studies<sup>51,52</sup> to exclude the adiabatic variations and show the real electron distribution along  $L^*$  (the inversion of the third adiabatic invariant in the adiabatic invariant coordinate). In addition, we use the ULF, ELF, and VLF wave data from the Electric and Magnetic Field Instrument Suite Integrated Science (EMFISIS) instrumentation suite<sup>53</sup> onboard both Van Allen Probes and the precipitating and trapped electron fluxes from the medium energy proton/electron detector (MEPED) onboard NOAA-POES 15, 16, 18, and 19 spacecraft, to further analyze the potential mechanisms of the electron PSD changes.

## III. OBSERVATION RESULTS

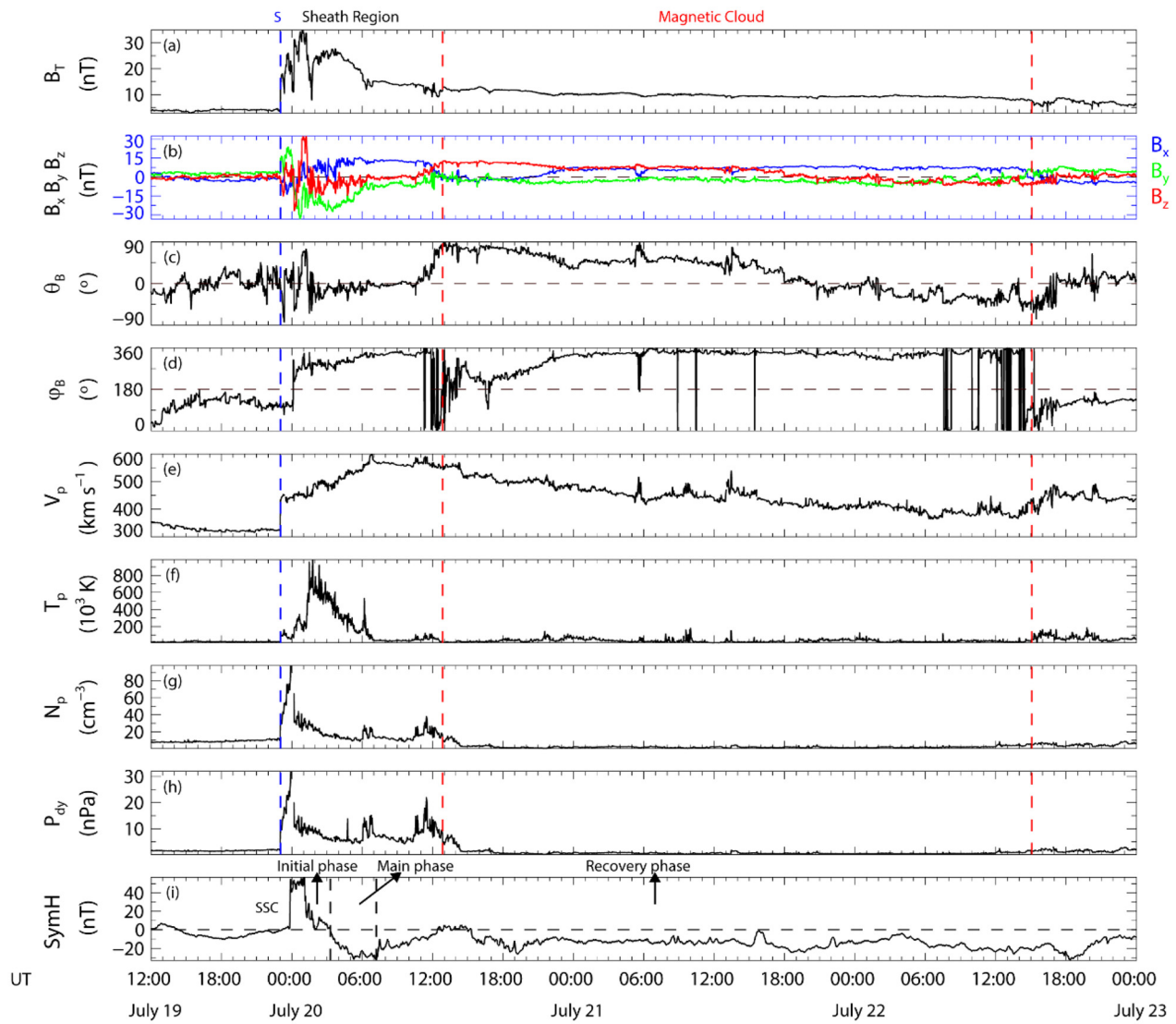
### A. MC event and the driven geomagnetic storm

Figure 1 shows an overview of the magnetic cloud event observed by WIND on 19–23 July 2016 and the driven geomagnetic storm.

A magnetic cloud event impinged the Earth's magnetosphere with the driven shock arriving at 23:02 UT on 19 July (see the blue vertical dashed line labeled by "S") with a distinct sharp enhancement of the magnitude of the magnetic field [Figs. 1(a) and 1(b)] and sudden increase in the plasma bulk velocity, proton temperature, and number density [Figs. 1(e)–1(g)]. After the shock, the turbulent sheath region succeeded featured by relatively stronger turbulent magnetic fields (see the region between the blue and the red vertical dashed lines). Notably, the solar wind dynamic pressure continued to increase with a peak value close to 30 nPa and stayed at a high level in the entire sheath region. The body of the magnetic cloud can be identified after 12:04 on 20 July (the first red vertical dashed line) by strong magnetic fields relative to solar wind with average of magnetic field magnitude of 9.83 nT [Fig. 1(a)], smooth rotation in the direction of magnetic fields with the latitudinal angle  $\theta$  varying from  $89.2^\circ$  to  $-60.8^\circ$  [Figs. 1(b)–1(d)] and exceptionally low proton temperature [Fig. 1(f)]. When the shock compressed the magnetosphere, the storm sudden commencement (SSC) was induced at 23:50 UT on June 19 July [Fig. 1(i)]. After that, a weak geomagnetic storm started with a minimum value of SymH of approximately  $-32$  nT. The main phase of the storm started at 03:18 UT and 07:12 UT on 20 July [the black vertical dashed lines in Fig. 1(j)]. The condition of the persistent high value of the dynamic pressure in the sheath region combined with the comparably weak geomagnetic storm provides a good opportunity to distinguish the sudden source and loss of the radiation belt electrons induced by the interplanetary shock and the subsequent sheath-driven weak storm.

### B. Temporal evolution of the electron fluxes during the MC event passage

Figures 2(a) and 2(b) show the time shifted dynamic pressure profile from Wind as well as the Dst, AE, and IMF-Bz index obtained from the Omni-web during the interval between 16:00 UT on 19 July and 16:00 UT on 20 July 2016. The corresponding flux evolution of the radiation belt electrons at  $90^\circ$  pitch angle at six selected energy channels from 54 keV to 2.6 MeV from REPT and MagEIS in Van Allen Probe-A and -B is illustrated in Figs. 2(c)–2(h). Overall, the temporal evolution of the electron fluxes experienced three stages. First, immediately after the IP shock (see the left red vertical dashed line), the magnitude of electron fluxes for all six energies had a notable enhancement with few orders followed by periodic oscillations as the dynamic pressure attempted to increase to  $\sim 10$  Pa and SymH up to  $\sim 55$  nT. A detailed investigation of this shock-induced radiation belt electron enhancement is provided in Fig. 4. Second, in the initial phase, the dynamic pressure continued to increase and arrived at its maximum when the electron fluxes at all six energies had an obvious dropout (between the first and the second red vertical dashed lines). After that, the electron fluxes had a clear dropout before the Dst index decreased to  $<-10$  nT. This significant sudden loss preferentially occurred at higher  $L$ -shells, indicating that the magnetopause shadowing effect may be responsible for the dropout event. Finally, in the storm main phase, the substorm also appeared triggered by the magnetic cloud when the AE index increased to  $>500$  nT, and the IMF-Bz was lower than 0, as shown in Fig. 2(b). The electrons at 54 and 108 keV were notably enhanced, which was likely due to substorm injections, while the fluxes of the electrons at energies  $>108$  keV basically stayed at low levels.



**FIG. 1.** An overview of the magnetic cloud event during 19–23 July 2016, including (a) magnetic field intensity and (b) its three components (in GSE), (c) latitudinal angle and (d) longitudinal angle, (e) plasma bulk velocity, (f) proton temperature, (g) number density, (h) solar wind dynamic pressure, and (i) SymH index. The shock is labeled with “S,” and the MC body is marked with the two red vertical dashed lines. The main phase of the MC-induced storm is also marked with two black vertical dashed lines in panel (i).

07 February 2024 05:48:15

### C. Evolution of electron PSD vs $L^*$

The temporal evolution of electron PSD vs  $L^*$  for relativistic electrons at  $\mu = 1584$  MeV/G (corresponding roughly to  $\sim 2.3$  MeV at  $L = 4.5$  or 3 MeV at  $L = 4.0$  for a dipole field) with  $K = 0.08 G^{1/2} R_E$  and  $K = 0.17 G^{1/2} R_E$  (corresponding to equatorial pitch angles of  $50^\circ$ – $60^\circ$  and  $30^\circ$ – $40^\circ$  for a dipole field) is shown in Figs. 3(a) and 3(b), respectively. In Fig. 3(a), when the IP shock arrived at 23:50 UT, VAP-B was located at  $L^* = 2.85$  in its inbound trajectory (curve 9), while VAP-A was at  $L^* = 4.2$  in its outbound trajectory (curve 10). Right after the shock, VAP-A (see curve 10) experienced a periodical increase in PSD at  $L^* < 5$  before witnessing a gradual decrease by electron drift echoes at  $L^* > 5$ , while dynamic pressure ( $P_{dyn}$ ) persistently

increased. This suggests that shock-induced electron injection could be responsible for the observed enhancement of the relativistic electron PSD at lower  $L$ -shells, while the continuous high dynamic pressure is the main driver of electron loss at high  $L$ -shells. As  $P_{dyn}$  continued to increase, both probes found a sharp PSD gradient at  $L^* = \sim 5$ . This suggests that the  $L^*$ -distributions of the relativistic electron PSD were redistributed by the magnetic cloud-driven IP shock and the following high dynamic pressure. In the storm main phase (after 3:17 UT), the PSD has a noticeable rapid loss at a broad spatial range of  $L$ -shells ( $L^* > 3$ ), shown as curves 13–18, suggesting a typical storm main phase dropout. Similar results can also be found in Fig. 3(b), although curves 10, 12, and 19 are not shown due to the lack of data below  $50^\circ$  pitch

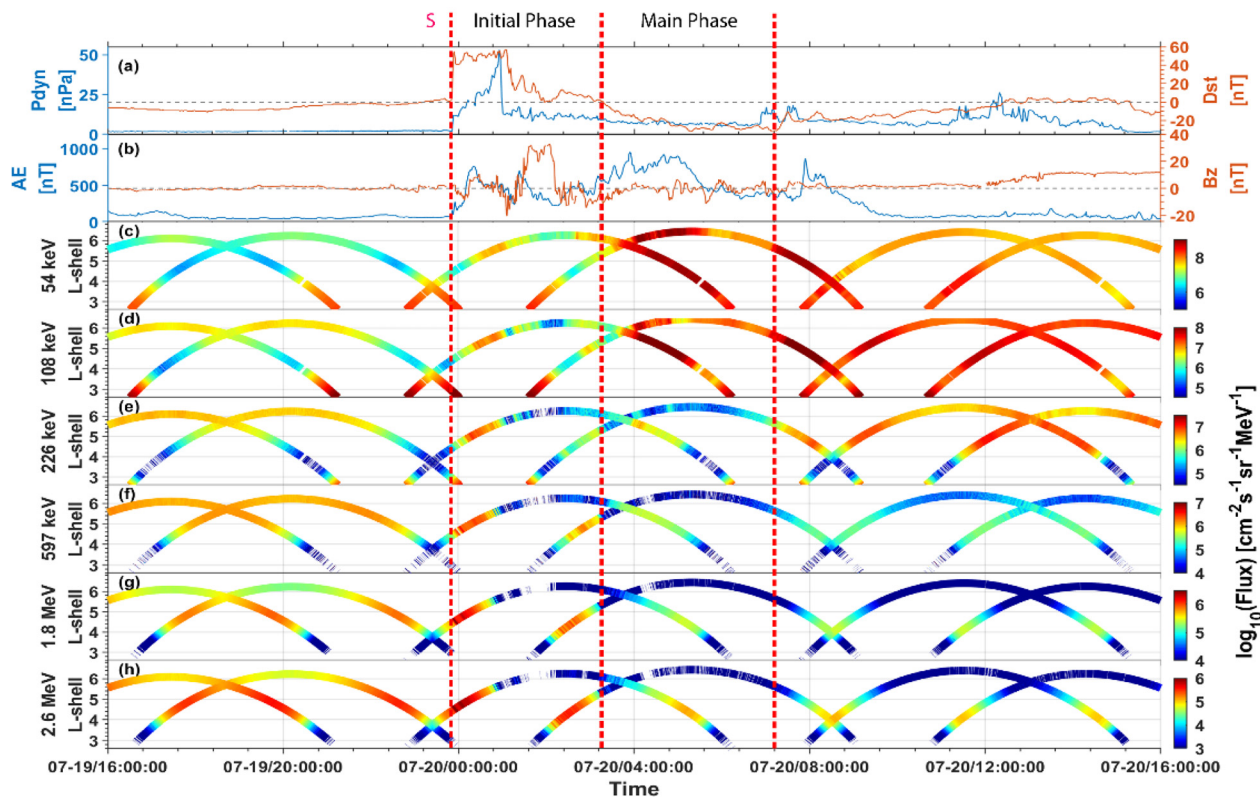


**FIG. 2.** An overview of radiation belt electron evolutions during 19–20 July 2016: (a) the dynamic pressure and Dst; (b) AE and IMF-Bz; (c)–(h) temporal evolutions of electron fluxes at  $90^\circ$  pitch angle for six specialized energies (from 54 keV to 2.6 MeV) at different L-shells measured by VAP-A and -B.

07 February 2024 05:48:15

angles. Therefore, it is clearly identified that the shock-induced rapid enhancement as well as high L-shell dropout of the relativistic electron PSD occurred in a broad range of pitch angles.

For electrons at lower energies, the PSD evolution responding to the magnetic cloud has drastic differences. The electrons at  $\mu = 100 \text{ MeV/G}$  (corresponding roughly to  $\sim 370 \text{ keV}$  at  $L = 4.5$ ) with  $K = 0.08 \text{ G}^{1/2} R_E$ , which we usually call “the seed electrons,” had a slight decrease after the IP shock, as shown in curves 9–11 in Fig. 3(c). Furthermore, the PSD at  $L > 4.5$  comparably increased when the storm main phase came, as shown in curves 12–18. This indicates that the main phase dropout was totally absent. For electrons at  $\mu = 10 \text{ MeV/G}$  (corresponding roughly to  $\sim 50 \text{ keV}$  at  $L = 4.5$ ) with  $K = 0.08 \text{ G}^{1/2} R_E$ , i.e., “the source electrons,” the PSD continued to increase during all stages of the MC event.

#### D. Possible source and loss processes

The electron flux at a  $90^\circ$  pitch angle for 15 energies from 54 to 1575 keV and 6 energies from 1.8 to 5.2 MeV measured by MagEIS and REPT in Van Allen Probe-A is illustrated in Fig. 4(f). The corresponding total magnitude ( $B_t$ ) of the geomagnetic field and magnitude of the electric field in the  $y$  and  $z$  directions under GSE coordinates from the EMFISIS and EFW instruments are shown in Figs. 4(c)–4(e). To better find the physical mechanism of shock-induced flux periodic oscillations, we zoom the GSE  $E_y$  and  $E_z$  in the time stamp from

23:50 UT on July 19 to 01:00 UT on July 20 in Fig. 4(g) and the 10-min residual flux spectrum in Fig. 4(h). For each energy and pitch angle channel, the residual flux  $(J - J_0)/J_0$  of energetic electrons is calculated, where  $J$  is the flux measured by MagEIS and  $J_0$  is its 10 min running-boxcar average.<sup>37</sup> The electric field in both the  $y$ - and  $z$ -components had a notable growth by 1–2 mV/m with the shock arrival, and the residual flux spectrogram showed a dispersion by energies. It is interesting that the period of flux echoes in each energy channel was approximately near their drift period rather than the electric field period. For instance, the time ellipse between the first two peaks of electron residual flux at 2.1 MeV was approximately 500 s when the probe went at  $L = \sim 4.5$ , as marked with a red arrow in Fig. 4(h). The value is in accordance with the calculated drift period in a dipole geomagnetic field in previous studies.<sup>35</sup> This suggests that the electric field cannot account for the modulation of electron oscillations. The possible scenario could be that the prompt increase in  $E_y$  and  $E_z$  triggers a one-kick enhancement. Note that the increase in electron fluxes between the two red vertical dashed lines was likely due to the growth of the total magnetic field ( $B_t$ ) by conserving the first adiabatic invariant.

To quantitatively trace the variations of electron PSD and analyze their potential variation mechanism(s), Fig. 5 (from top to bottom) shows the dynamic pressure, Dst, AE, and  $B_z$  indices, the estimated minimum locations of the magnetopause (MP) calculated by Shue *et al.*<sup>34</sup> and of the last closed drift shell (LCDS) of relativistic electrons

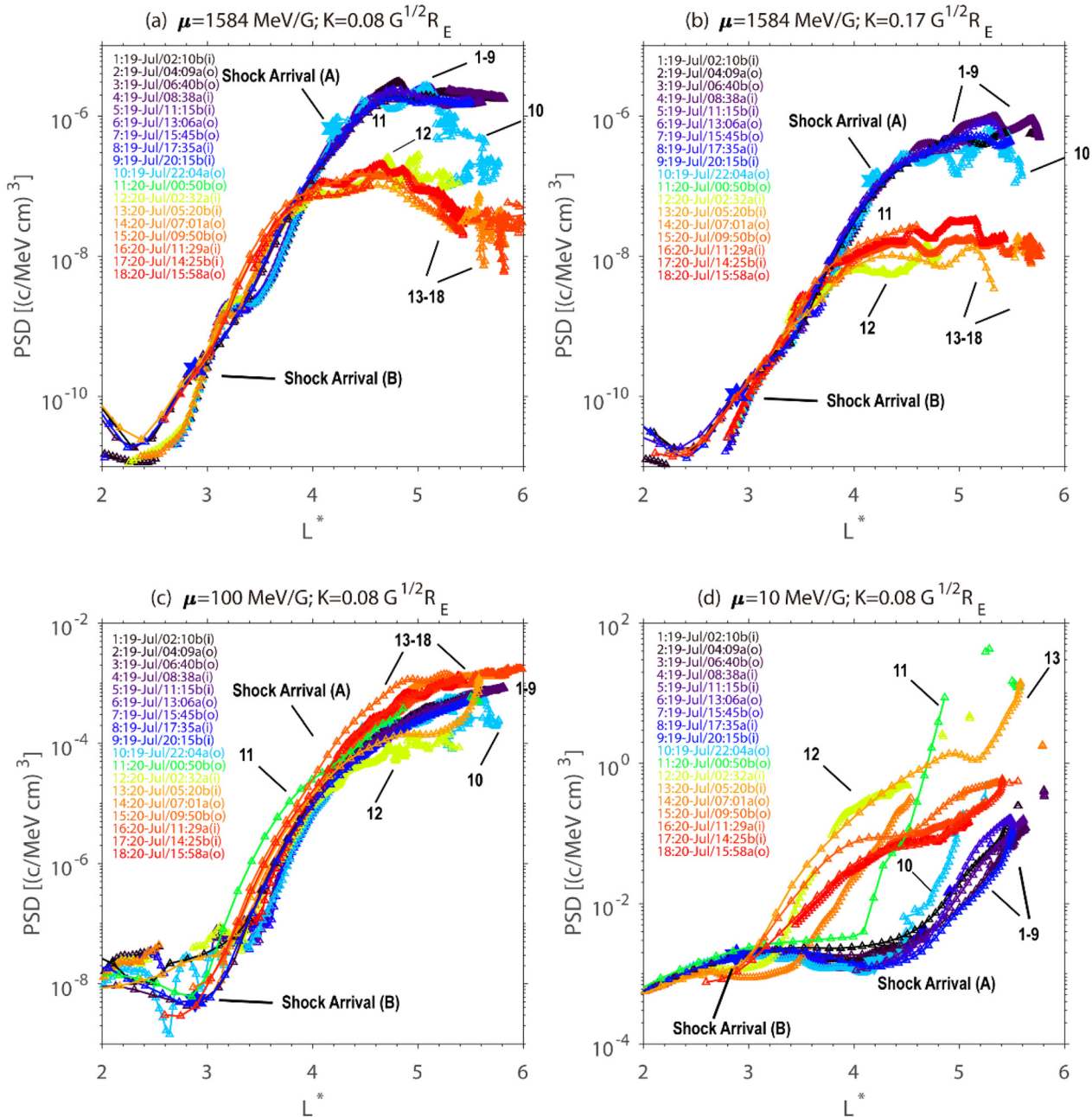


**FIG. 3.** PSD distributions as a function of  $L^*$  for relativistic electrons with  $\mu = 1584 \text{ MeV}/\text{G}$  and (a)  $K = 0.08 \text{ G}^{1/2}R_E$  and (b)  $K = 0.17 \text{ G}^{1/2}R_E$ . PSD distributions for (c) seed electron with  $\mu = 100 \text{ MeV}/\text{G}$  and (d) source electron with  $\mu = 10 \text{ MeV}/\text{G}$ . Various colors correspond to different inbound or outbound orbit passes from VAP-A (squares) and VAP-B (triangles), with the start time of each pass (o: outbound; i: inbound) labeled. Each curve is numbered for ease of identification.

for  $K = 0.17$  [Fig. 5(c)] from the LANLGeoMag library,<sup>55</sup> and the temporal evolution of electron PSD at  $\mu = 1584 \text{ MeV}/\text{G}$  with  $K = 0.17 \text{ MeV}/\text{G}$  [Figs. 5(d) and 5(e)] and  $K = 0.08 \text{ MeV}/\text{G}$  [Figs. 5(f)–5(g)]. Similar to the results in a previous study,<sup>23</sup> sustained high dynamic pressure can drive the MP and LCDS inward, inducing electron dropout at  $L^* > 5$ . Additionally, the rapid loss in the storm main phase appeared when the

LCDS moved to lower  $L^*$  ( $L^* < 7$  or even to  $L^* = 5$ ) by the increase in the southward IMF- $B_s$  and the growth of the AE index from a few nT to  $> 1000$  nT. The trapped and precipitating electron fluxes at  $> 1 \text{ MeV}$  measured by NOAA-POES 15, 16, 18, and 19 spacecraft are also shown in Figs. 5(h)–5(i). During the whole event, the precipitating electrons experienced no distinct increase compared with the trapped electron

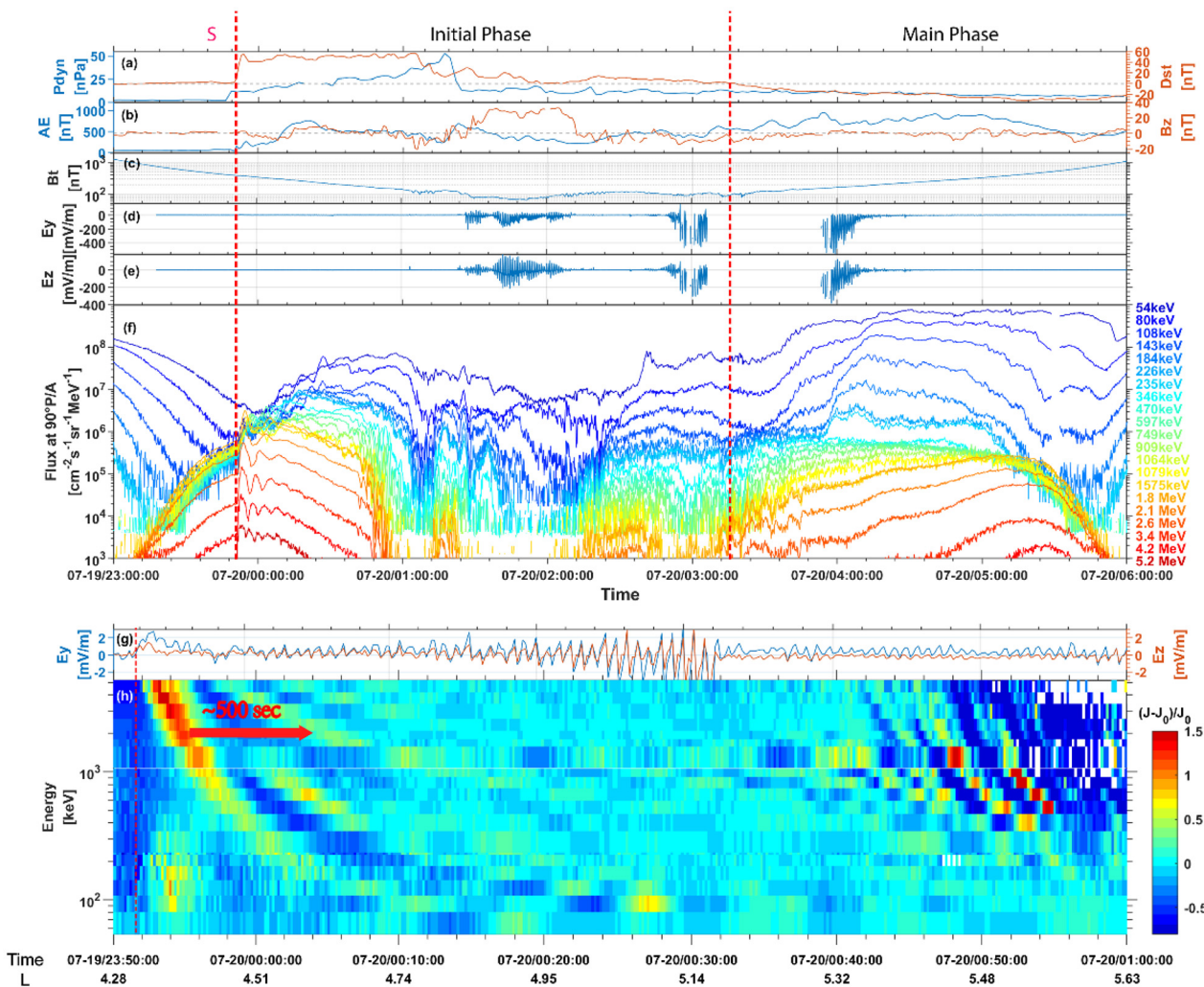


**FIG. 4.** (a) and (b)  $P_{\text{dyn}}$ , Dst, AE, and IMF- $B_z$ ; (c) magnitude of the total geomagnetic field; (d)–(e)  $y$  and  $z$  components of the total electric field; (f) temporal evolutions of electron fluxes at  $90^\circ$  pitch angle at 21 energies from 54 keV to 5.2 MeV; (g)  $E_y$  and  $E_z$ , and (h) spectrum of residual flux at the time period around the IP shock (marked with a red vertical line). The time eclipse between the first two peaks for 2.1 MeV electron residual flux is marked with a red arrow in Fig. 4(h).

fluxes, providing evidence that the observed electrons rarely precipitated into the atmosphere by wave-particle interactions.

Figures 6(a) and 6(b) show the temporal evolutions of the magnetic intensity of ULF waves in the Pc5 frequency range, which is comparable to the drift period of relativistic electrons (e.g., electrons at 1 MeV with a drift period of approximately 10 min) measured by both Van Allen Probes. The ULF waves became remarkably intense after the SSC and maintained a high magnitude during the storm main phase. Their potential capability of driving radiation belt energetic electrons outward transport can help the electron PSD dropout processes. When magnetic clouds impinge on the Earth's magnetosphere, charged electrons and ions injected via magnetic reconnections can be trapped in the radiation belt. Kinds of instability could potentially generate a variety of plasma waves that have capabilities for scattering electrons in the Earth's radiation belt. The magnetic intensity of ELF waves ( $<10$  Hz) and VLF waves (10–10 000 Hz) is shown in Figs. 6(c)–6(f).

First, the EMIC waves, which are capable of precipitating high-energy radiation belt electrons to the atmosphere within  $<1$  h, can be found in Figs. 6(c) and 6(d) by both spacecraft. However, they mainly appeared at high L-shells ( $>5.5$ ), and no obvious local depletions of electron PSD can be found in Fig. 5. Considering the absence of the precipitation electrons measured by NOAA-POES in Fig. 5 and the intense ULF waves present in Figs. 6(a) and 6(b), a conclusion could be given that the electron dropout event is induced by magnetopause shadowing combined with ULF wave-led outward transport rather than local loss by wave-particle interactions. Second, chorus waves were clearly observed before and during the storm main phase. It is suggested that chorus wave-induced wave-particle interactions may contribute to the source process of relativistic electrons during the main phase. In addition, the plasmaspheric hiss (blue) and MS waves (black), which were also present during this event, can hardly rapidly deplete radiation belt electrons within a few hours.

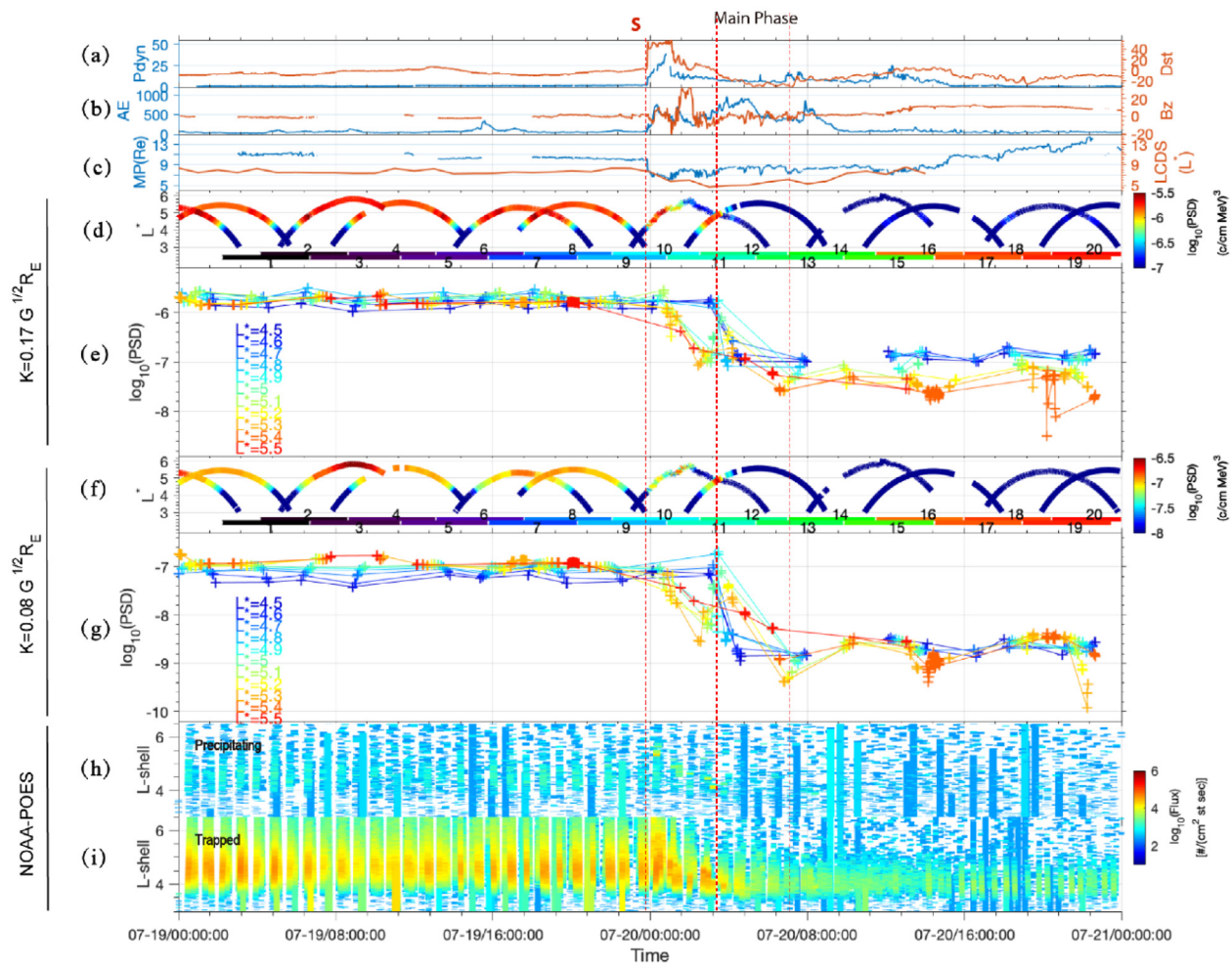


**FIG. 5.** Temporal evolutions of electron PSD distributions during 19–21 July 2016: (a) and (b)  $P_{dyn}$ , Dst, AE, and IMF- $B_z$ ; (c) magnetopause location (MP) and LCDS; (d) electron PSD vs  $L^*$  and (e) color-coded temporal evolution of electron PSD at  $K = 0.17 G^{1/2}R_E$  and  $\mu = 1584 \text{ MeV/G}$  (the inbound and outbound passes are marked as in Fig. 3); (f) electron PSD vs  $L^*$  and (g) color-coded temporal evolution of electron PSD at  $K = 0.08 G^{1/2}R_E$  and  $\mu = 1584 \text{ MeV/G}$ ; and (h)–(i) spectra of precipitating and trapped electron flux from NOAA-POES 15, 16, 18, and 19 at  $E_k > 1 \text{ MeV}$ .

### E. Quantitative equilibrium lines between source and loss processes

Figures 7(a)–7(c) show the ratio of the PSD change for electrons at various  $\mu$  ranging from  $10^\circ$  to  $10^4 \text{ MeV/G}$  with a constant  $K = 0.08 G^{1/2}R_E$  observed by both probes during three stages. The ratio was calculated as follows:

$$\text{ratio} = PSD_{\text{current}} / PSD_{\text{before}} \quad (1)$$

where  $PSD_{\text{before}}$  is the averaged electron PSD before the solar wind event (curves 1–9 in Fig. 3).  $PSD_{\text{current}}$  is the electron PSD at “after the shock” (curves 10–11 in Fig. 3), “storm the main phase” (curves 12–13 in Fig. 3), and “storm recovery phase” (curves 14–17 in Fig. 3) as listed in Table I. After the shock, the value of PSD at  $L^* > 5$  increased by  $>1$  order of magnitude for electrons at  $\mu < \sim 10^{1.5} \text{ MeV/G}$ . The likely reason would be that these “source electrons” were injected from the magnetotail via magnetic connection as well as inward transportation

processes, which is frequently observed and discussed in previous studies. Comparably, the “relativistic electrons” and “higher energy seed electrons” ( $\mu > 10^{1.5} \text{ MeV/G}$ ) experienced a prompt enhancement at  $L^* = 4$ –5 and a decrease at  $L^* > 5$ , which can also be found in Figs. 3 and 4. Here, we mark  $10^{1.5} \text{ MeV/G}$  (the horizontal dashed lines) for electrons at higher  $L^*$  ( $L^* > 4$ ) as the energy equilibrium edge as well as the  $L^* = 5$  and  $L^* = 4$  (the vertical dashed lines) spatial location equilibrium edges. During the storm main phase, as the substorm intensified, the injection source electrons penetrated to lower  $L^*$  up to  $L^* < 3.5$  and could be accelerated to higher energies, i.e., near  $100 \text{ MeV/G}$ , while the dropout for seed and relativistic electrons became pronounced, as shown in Figs. 3 and 5. The growth of PSD at  $L^* = 3$ –4 for electrons at  $\mu > \sim 100 \text{ MeV/G}$  potentially accounts for some inward radial diffusion mechanism during the main phase. During the storm recovery phase, the equilibrium edge continued moving to high energies, which could be due to the intensity of the

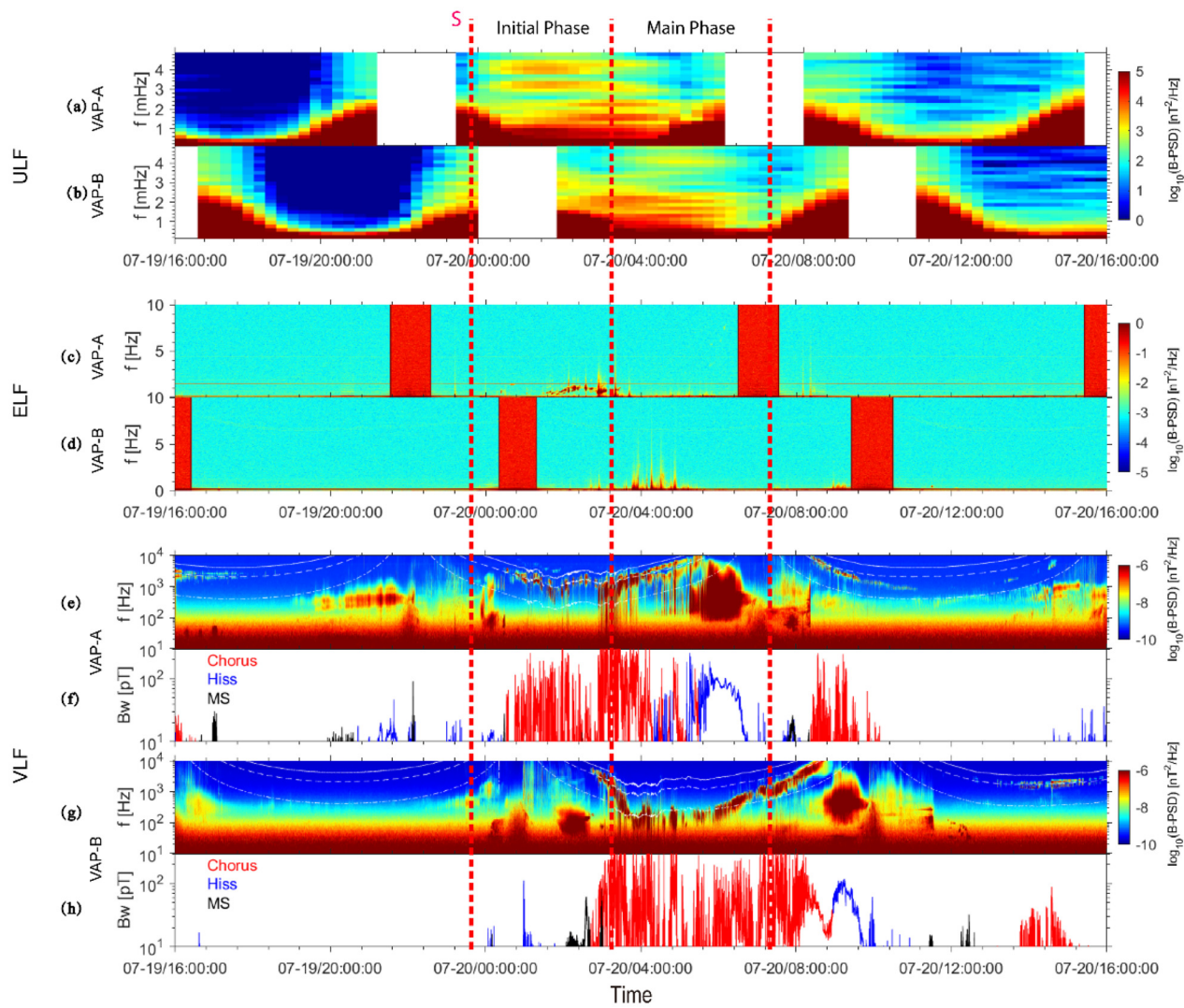


**FIG. 6.** Temporal evolutions of the magnetic power spectral density (B-PSD) of (a) and (b) ULF waves at 1–5 mHz; (c) and (d) ELF waves at 0–10 Hz; and (e) and (g) VLF waves at 10<sup>1</sup>–10<sup>4</sup> Hz as well as (f) and (h) the amplitude ( $B_w$ ) of the identified whistler-mode chorus (red), plasmaspheric hiss (blue), and magnetosonic (MS) waves (black) observed from VAP-A and VAP-B, respectively.

energization process dominated by the whistler-mode chorus. However, for electrons at  $E_k > 10^{2.5}$  keV, the equilibrium edge is almost constant at  $L^* = \sim 4$ , suggesting that the weakness of the geomagnetic storm as well as substorms rarely influenced the distributions of the relativistic and sub-relativistic electrons. To better compare the profile change in the electron PSD distribution during different stages of the storm, Figs. 7(d)–7(g) show the electron PSD vs  $\mu$  at four typical locations. At  $L^* = 3.5$ , the value of PSD for electrons at all energies had almost similar profiles during different storm stages. At  $L^* = 4.0$ , the PSD at  $\mu < \sim 100$  MeV/G had a clear increase during the main phase and recovery phase, while the PSD at  $\mu > \sim 100$  MeV/G had a very slight increase. In the core of the radiation belt, i.e., at  $L^* = 4.5$ , the PSD at  $\mu > \sim 100$  MeV/G had a significant drop compared with that at  $L^* = 4$ . This means that  $\mu = \sim 100$  MeV/G is a typical value for

electron dynamic equilibrium. At  $L^* = 5.4$ , which is near the outer observational limit of the probes, the relativistic electrons keep decreasing during the whole event, while the electron seed and source electrons are enhanced during the main phase before having a slight decrease, which is similar to Fig. 7(c). Overall, it could be concluded that the loss processes were competing with the source processes, which are strongly sensitive to electron energy and L-shells.  $L^* = \sim 4$  and  $\mu = 10^2$ – $10^{2.5}$  MeV/G could be typical values at which the source and loss processes arrived at dynamic equilibrium. Both observations and simulations suggest that solar wind influences radiation belt particles in a direct way, e.g., compression of the magnetosphere by high dynamic pressure, and in an indirect way, e.g., wave-particle interactions controlled by plasma waves that are excited by ejected particles. Therefore, the balance lines in electron energies and  $L^*$  also provide

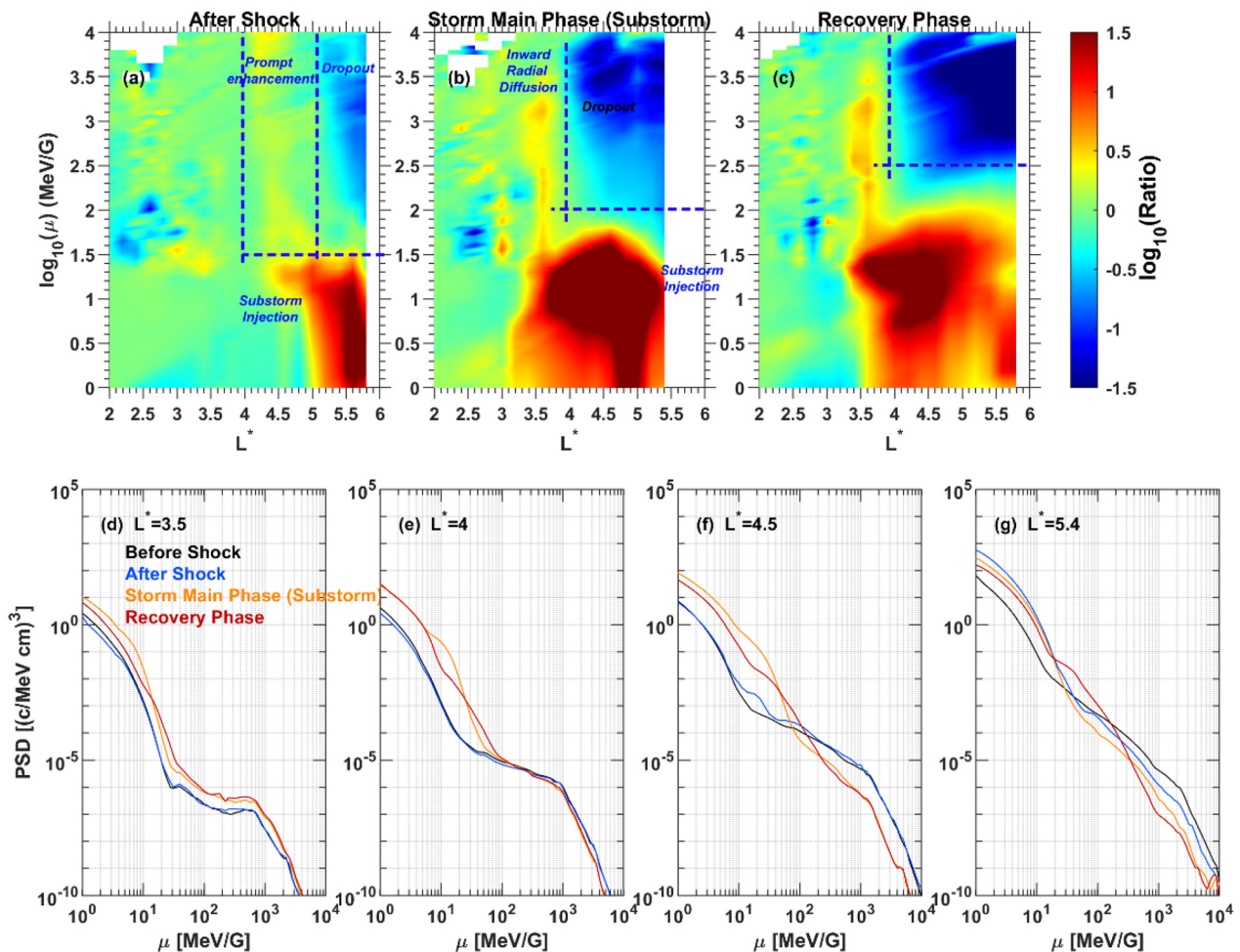


**FIG. 7.** (a)–(c) The ratio of the PSD change for electrons at  $\mu = 10^0 - 10^4$  MeV/G with  $K = 0.08 G^{1/2} R_E$  observed by both probes during different stages of the event. (d)–(g) Distribution of the electron PSD at  $\mu = 10^0 - 10^4$  MeV/G with  $K = 0.08 G^{1/2} R_E$  before the shock, after shock, storm main phase, and recovery phase, respectively.

**TABLE I.** The Numerator  $PSD_{\text{current}}$  in Eq. (1): electron PSD at after the shock (curve 10 for VAP-A and 11 for VAP-A in Fig. 3), storm main phase (curve 12 for VAP-A and 13 for VAP-B in Fig. 3), and storm recovery phase (curve 14 for VAP-A and 17 for VAP-B in Fig. 3).

	After shock (Substorm)	Storm main phase	Storm recovery phase
VAP-A	Curve 10	Curve 12	Curves 14, 16, and 18
VAP-B	Curve 11	Curve 13	Curves 15 and 17

new and comprehensive insight into both direct and indirect disturbances from solar winds.

#### IV. SUMMARY

In this investigation, we report and discuss the competition between source and loss processes under extremely high values of dynamic pressure in the magnetic cloud sheath region combined with

a comparably weak geomagnetic storm driven by magnetic clouds. The detailed analysis demonstrates that the competition between the source and loss processes of the radiation belt electrons is highly sensitive to electron energy and spatial locations during different stages of magnetic cloud–magnetosphere coupling. The main conclusions can be summarized as follows:

- (1) For relativistic electrons, the energization process occurred at the lower  $L$ -shells immediately after MC-driven shock, while the magnetopause shadowing combined outward transportation effect dominated the dropout at higher  $L$ -shells.
- (2) For seed electrons, both magnetopause shadowing-led loss processes and whistler-mode chorus-led accelerations competed, resulting in comparable slight changes.
- (3) For source electrons, the substorm injections cause a distinct electron to increase at the outer edge of the radiation belt after the shock and penetrate into a deeper location during the storm main phase.
- (4)  $L^* = \sim 4$  and  $\mu = 10^2 - 10^{2.5}$  MeV/G can be the balance lines at which the source and loss processes arrive in dynamic equilibrium.

The source and loss processes of radiation belt electrons always occur simultaneously and mainly originate from the coupling between the solar wind and the Earth's magnetosphere. In this study, we first quantitatively give the balance lines in energy channels and  $L^*$  at which both processes arrived at a dynamic equilibrium for source, seed, and relativistic electrons. The balance lines could be a key factor, which is valuable for special consideration when investigating radiation belt dynamics in the future. Note that the calculated balance lines would theoretically and predictably change since the temporal evolution of radiation belt electrons has been proven case-by-case during the interaction of solar wind disturbances and the magnetosphere. In the subsequent work, we will discuss and provide statistical investigations of the temporospatial distributions of the balance lines of the radiation belt electrons in response to different solar wind disturbances. In addition, the protons and other heavy ions (such as helium and oxygen) that are trapped within the inner magnetosphere preferentially contribute to the formation of the inner radiation belt and the ring current. However, the quantitative analysis of the dynamic equilibrium of their source and loss effects caused by magnetic cloud events has been barely addressed. In the future study, we will compare the flux and PSD changes of these ions during different stages of magnetic cloud events.

## ACKNOWLEDGMENTS

This work was jointly supported by the National Key Research and Development Program of China (Grant No. 2022YFF0503904), the National Natural Science Foundation of China (Grant Nos. 42074205 and 12250014), and the Science and Technology Development Fund of Macao SAR (File No. 0048/2021/A). The wind MFI and SWE data and geomagnetic indices are available at NASA OmniWeb (<http://cdaweb.gsfc.nasa.gov>). The REPT and MagEIS data are obtained from <https://spdf.gsfc.nasa.gov/pub/data/rbsp>. The EMFISIS data are derived from <https://emfisis.physics.uiowa.edu/data/index>. The NOAA-POES data are downloaded from <https://spdf.gsfc.nasa.gov/pub/data/noaa/>.

## AUTHOR DECLARATIONS

### Conflict of Interest

The authors have no conflicts to disclose.

### Author Contributions

**Zhengyang Zou:** Conceptualization (equal); Data curation (equal); Formal analysis (equal); Funding acquisition (equal); Investigation (equal); Methodology (equal); Project administration (equal); Resources (equal); Software (equal); Supervision (equal); Validation (equal); Visualization (equal); Writing – original draft (equal); Writing – review & editing (equal). **Pingbing Zuo:** Conceptualization (equal); Funding acquisition (equal); Investigation (equal); Methodology (equal); Writing – original draft (equal); Writing – review & editing (equal). **Binbin Ni:** Conceptualization (equal); Funding acquisition (equal); Methodology (equal); Project administration (equal); Writing – original draft (equal); Writing – review & editing (equal). **Jiayun Wei:** Data curation (equal); Formal analysis (equal); Funding acquisition (equal); Validation (equal); Visualization (equal); Writing – original draft (equal). **Wentao Zhou:** Validation (equal); Visualization (equal); Writing – original

draft (equal); Writing – review & editing (equal). **Hanyu Huang:** Validation (equal); Visualization (equal); Writing – original draft (equal); Writing – review & editing (equal). **Yanqiong Xie:** Methodology (equal); Software (equal); Writing – review & editing (equal).

## DATA AVAILABILITY

The data that support the findings of this study are available from the corresponding author upon reasonable request.

## REFERENCES

- <sup>1</sup>D. N. Baker, S. G. Kanekal, V. C. Hoxie, M. G. Henderson, X. Li, H. E. Spence, S. R. Elkington, R. H. Friedel, J. Goldstein, M. K. Hudson, G. D. Reeves, R. M. Thorne, C. A. Kletzing, and S. G. Claudepierre, "A long-lived relativistic electron storage ring embedded in Earth's outer Van Allen belt," *Science* **340**(6129), 186–190 (2013).
- <sup>2</sup>B. Ni, Y. Shprits, M. Hartinger, V. Angelopoulos, X. Gu, and D. Larson, "Analysis of radiation belt energetic electron phase space density using THEMIS SST measurements: Cross-satellite calibration and a case study," *J. Geophys. Res.* **116**(A3), A03208, <https://doi.org/10.1029/2010JA016104> (2011).
- <sup>3</sup>B. Ni, Z. Zou, X. Gu, C. Zhou, R. M. Thorne, J. Bortnik, R. Shi, Z. Zhao, D. N. Baker, S. G. Kanekal, H. E. Spence, G. D. Reeves, and X. Li, "Variability of the pitch angle distribution of radiation belt ultrarelativistic electrons during and following intense geomagnetic storms: Van Allen Probes observations," *J. Geophys. Res.* **120**(6), 4863–4876, <https://doi.org/10.1002/2015JA021065> (2015).
- <sup>4</sup>R. M. Thorne, B. Ni, X. Tao, R. B. Horne, and N. P. Meredith, "Scattering by chorus waves as the dominant cause of diffuse auroral precipitation," *Nature* **467**(7318), 943–946 (2010).
- <sup>5</sup>D. L. Turner, V. Angelopoulos, S. K. Morley, M. G. Henderson, G. D. Reeves, W. Li, D. N. Baker, C.-L. Huang, A. Boyd, H. E. Spence, S. G. Claudepierre, J. B. Blake, and J. V. Rodriguez, "On the cause and extent of outer radiation belt losses during the 30 September 2012 dropout event," *J. Geophys. Res.* **119**(3), 1530–1540, <https://doi.org/10.1002/2013JA019446> (2014).
- <sup>6</sup>F. He, R.-L. Guo, W. R. Dunn, Z.-H. Yao, H.-S. Zhang, Y.-X. Hao, Q.-Q. Shi, Z.-J. Rong, J. Liu, A.-M. Tian, X.-X. Zhang, Y. Wei, Y.-L. Zhang, Q.-G. Zong, Z.-Y. Pu, and W.-X. Wan, "Plasmapause surface wave oscillates the magnetosphere and diffuse aurora," *Nat. Commun.* **11**(1), 1668 (2020).
- <sup>7</sup>X.-Y. Wang, Q.-H. Zhang, C. Wang, Y.-L. Zhang, B.-B. Tang, Z.-Y. Xing, K. Oksavik, L. R. Lyons, M. Lockwood, Q.-G. Zong, G.-J. Li, J. Liu, Y.-Z. Ma, and Y. Wang, "Unusual shrinkage and reshaping of Earth's magnetosphere under a strong northward interplanetary magnetic field," *Commun. Earth Environ.* **4**(1), 31 (2023).
- <sup>8</sup>H. Fu, C. Yue, Q.-G. Zong, X.-Z. Zhou, and S. Fu, "Statistical characteristics of substorms with different intensity," *J. Geophys. Res.* **126**(8), e2021JA029318, <https://doi.org/10.1029/2021JA029318> (2021).
- <sup>9</sup>C. Katsavriias, I. A. Daglis, D. L. Turner, I. Sandberg, C. Papadimitriou, M. Georgiou, and G. Balasis, "Nonstorm loss of relativistic electrons in the outer radiation belt," *Geophys. Res. Lett.* **42**(24), 10,521–10,530, <https://doi.org/10.1002/2015GL066773> (2015).
- <sup>10</sup>X. Li, D. N. Baker, S. G. Kanekal, M. Looper, and M. Temerin, "Long term measurements of radiation belts by SAMPEX and their variations," *Geophys. Res. Lett.* **28**(20), 3827–3830, <https://doi.org/10.1029/2001GL013586> (2001).
- <sup>11</sup>G. D. Reeves, K. L. McAdams, R. H. W. Friedel, and T. P. O'Brien, "Acceleration and loss of relativistic electrons during geomagnetic storms," *Geophys. Res. Lett.* **30**(10), 1529, <https://doi.org/10.1029/2002GL016513> (2003).
- <sup>12</sup>R. M. Thorne, W. Li, B. Ni, Q. Ma, J. Bortnik, L. Chen, D. N. Baker, H. E. Spence, G. D. Reeves, M. G. Henderson, C. A. Kletzing, W. S. Kurth, G. B. Hospodarsky, J. B. Blake, J. F. Fennell, S. G. Claudepierre, and S. G. Kanekal, "Rapid local acceleration of relativistic radiation-belt electrons by magnetospheric chorus," *Nature* **504**(7480), 411–414 (2013).
- <sup>13</sup>L. Luo, X. Xu, Y. Zhang, Z. Zhou, Q. Chang, Q. Xu, X. Wang, P. He, S. Yi, and H. Li, "The three-fluid generalized Ohm's law: A theoretical study," *Phys. Fluids* **35**(1), 017134 (2023).

- <sup>14</sup>Y. Ji, C. Shen, L. Ma, N. Ren, and N. Ahmad, "Statistics of geometrical invariants of magnetic field gradient tensors in the turbulent magnetosheath based on magnetospheric multiscale mission," *Phys. Fluids* **35**(2), 025107 (2023).
- <sup>15</sup>D. Wang, Y. Y. Shprits, I. S. Zhelavskaya, F. Effenberger, A. M. Castillo, A. Y. Drozdov, N. A. Aseev, and S. Cervantes, "The effect of plasma boundaries on the dynamic evolution of relativistic radiation belt electrons," *J. Geophys. Res.* **125**(5), e2019JA027422, <https://doi.org/10.1029/2019JA027422> (2020).
- <sup>16</sup>D. Wang and Y. Y. Shprits, "On how high-latitude chorus waves tip the balance between acceleration and loss of relativistic electrons," *Geophys. Res. Lett.* **46**(14), 7945–7954, <https://doi.org/10.1029/2019GL082681> (2019).
- <sup>17</sup>K.-C. Kim and D.-Y. Lee, "Magnetopause structure favorable for radiation belt electron loss," *J. Geophys. Res.* **119**(7), 5495–5508, <https://doi.org/10.1002/2014JA019880> (2014).
- <sup>18</sup>Y. Y. Shprits, N. P. Meredith, and R. M. Thorne, "Parameterization of radiation belt electron loss timescales due to interactions with chorus waves," *Geophys. Res. Lett.* **34**(11), L11110, <https://doi.org/10.1029/2006GL029050> (2007).
- <sup>19</sup>Z. Su, H. Zhu, F. Xiao, Q. G. Zong, X. Z. Zhou, H. Zheng, Y. Wang, S. Wang, Y. X. Hao, Z. Gao, Z. He, D. N. Baker, H. E. Spence, G. D. Reeves, J. B. Blake, and J. R. Wygant, "Ultra-low-frequency wave-driven diffusion of radiation belt relativistic electrons," *Nat. Commun.* **6**, 10096 (2015).
- <sup>20</sup>D. L. Turner, Y. Shprits, M. Hartinger, and V. Angelopoulos, "Explaining sudden losses of outer radiation belt electrons during geomagnetic storms," *Nat. Phys.* **8**(3), 208–212 (2012).
- <sup>21</sup>D. L. Turner, V. Angelopoulos, W. Li, J. Bortnik, B. Ni, Q. Ma, R. M. Thorne, S. K. Morley, M. G. Henderson, G. D. Reeves, M. Usanova, I. R. Mann, S. G. Claudepierre, J. B. Blake, D. N. Baker, C.-L. Huang, H. Spence, W. Kurth, C. Kletzing, and J. V. Rodriguez, "Competing source and loss mechanisms due to wave-particle interactions in Earth's outer radiation belt during the 30 September to 3 October 2012 geomagnetic storm," *J. Geophys. Res.* **119**(3), 1960–1979, <https://doi.org/10.1002/2014JA019770> (2014).
- <sup>22</sup>D. L. Turner and A. Y. Ukhorskiy, "Outer radiation belt losses by magnetopause incursions and outward radial transport: New insight and outstanding questions from the Van Allen Probes era," in *The Dynamic Loss of Earth's Radiation Belts* (Elsevier, 2020), pp. 1–28.
- <sup>23</sup>Z. Zou, P. Zuo, B. Ni, Z. Gao, G. Wang, Z. Zhao, X. Feng, and F. Wei, "Two-step dropouts of radiation belt electron phase space density induced by a magnetic cloud event," *Astrophys. J. Lett.* **895**(1), L24 (2020).
- <sup>24</sup>C. Medeiros, V. M. Souza, L. E. A. Vieira, D. G. Sibeck, A. J. Halford, S.-B. Kang, L. A. D. Silva, L. R. Alves, J. P. Marchez, R. S. Dallaqua, P. R. Jauer, M. Rockenbach, O. Mendes, M. V. Alves, A. D. Lago, M.-C. Fok, S. G. Kanekal, D. N. Baker, and C. A. Kletzing, "On the contribution of EMIC waves to the reconfiguration of the relativistic electron butterfly pitch angle distribution shape on 2014 September 12—A case study," *Astrophys. J.* **872**(1), 36 (2019).
- <sup>25</sup>B. Ni, J. Bortnik, R. M. Thorne, Q. Ma, and L. Chen, "Resonant scattering and resultant pitch angle evolution of relativistic electrons by plasmaspheric hiss," *J. Geophys. Res.* **118**(12), 7740–7751, <https://doi.org/10.1002/2013JA019260> (2013).
- <sup>26</sup>D. Summers, B. Ni, and N. P. Meredith, "Timescales for radiation belt electron acceleration and loss due to resonant wave-particle interactions: 1. Theory," *J. Geophys. Res.* **112**(A4), A04206, <https://doi.org/10.1029/2006JA011801> (2007).
- <sup>27</sup>D. Summers, B. Ni, and N. P. Meredith, "Timescales for radiation belt electron acceleration and loss due to resonant wave-particle interactions: 2. Evaluation for VLF chorus, ELF hiss, and electromagnetic ion cyclotron waves," *J. Geophys. Res.* **112**(A4), A04207, <https://doi.org/10.1029/2006JA011993> (2007).
- <sup>28</sup>M. E. Usanova, A. Drozdov, K. Orlova, I. R. Mann, Y. Shprits, M. T. Robertson, D. L. Turner, D. K. Milling, A. Kale, D. N. Baker, S. A. Thaller, G. D. Reeves, H. E. Spence, C. Kletzing, and J. Wygant, "Effect of EMIC waves on relativistic and ultrarelativistic electron populations: Ground-based and Van Allen Probes observations," *Geophys. Res. Lett.* **41**(5), 1375–1381, <https://doi.org/10.1002/2013GL059024> (2014).
- <sup>29</sup>Z. Yuan, Y. Xiong, D. Wang, M. Li, X. Deng, A. G. Yahnnin, T. Raita, and J. Wang, "Characteristics of precipitating energetic ions/electrons associated with the wave-particle interaction in the plasmaspheric plume," *J. Geophys. Res.* **117**(A8), A08324, <https://doi.org/10.1029/2012JA017783> (2012).
- <sup>30</sup>Y. Y. Shprits, H. J. Allison, D. Wang, A. Drozdov, M. Szabo-Roberts, I. Zhelavskaya, and R. Vasile, "A new population of ultra-relativistic electrons in the outer radiation zone," *J. Geophys. Res.* **127**(5), e2021JA030214, <https://doi.org/10.1029/2021JA030214> (2022).
- <sup>31</sup>J. E. Borovsky, R. H. W. Friedel, and M. H. Denton, "Statistically measuring the amount of pitch angle scattering that energetic electrons undergo as they drift across the plasmaspheric drainage plume at geosynchronous orbit," *J. Geophys. Res.* **119**(3), 1814–1826, <https://doi.org/10.1002/2013JA019310> (2014).
- <sup>32</sup>J. E. Borovsky and M. H. Denton, "Relativistic-electron dropouts and recovery: A superposed epoch study of the magnetosphere and the solar wind," *J. Geophys. Res.* **114**(A2), A02201, <https://doi.org/10.1029/2008JA013128> (2009).
- <sup>33</sup>Y. X. Hao, Q. G. Zong, X. Z. Zhou, S. Y. Fu, R. Rankin, C. J. Yuan, A. T. Y. Lui, H. E. Spence, J. B. Blake, D. N. Baker, and G. D. Reeves, "Electron dropout echoes induced by interplanetary shock: Van Allen Probes observations," *Geophys. Res. Lett.* **43**(11), 5597–5605, <https://doi.org/10.1002/2016GL069140> (2016).
- <sup>34</sup>X.-J. Zhang, W. Li, R. M. Thorne, V. Angelopoulos, Q. Ma, J. Li, J. Bortnik, Y. Nishimura, L. Chen, D. N. Baker, G. D. Reeves, H. E. Spence, C. A. Kletzing, W. S. Kurth, G. B. Hospodarsky, J. B. Blake, and J. F. Fennell, "Physical mechanism causing rapid changes in ultrarelativistic electron pitch angle distributions right after a shock arrival: Evaluation of an electron dropout event," *J. Geophys. Res.* **121**(9), 8300–8316, <https://doi.org/10.1002/2016JA022517> (2016).
- <sup>35</sup>J. C. Foster, J. R. Wygant, M. K. Hudson, A. J. Boyd, D. N. Baker, P. J. Erickson, and H. E. Spence, "Shock-induced prompt relativistic electron acceleration in the inner magnetosphere," *J. Geophys. Res.* **120**(3), 1661–1674, <https://doi.org/10.1002/2014JA020642> (2015).
- <sup>36</sup>X. Li, I. Roth, M. Temerin, J. R. Wygant, M. K. Hudson, and J. B. Blake, "Simulation of the prompt energization and transport of radiation belt particles during the March 24, 1991 SSC," *Geophys. Res. Lett.* **20**(22), 2423–2426, <https://doi.org/10.1029/93GL02701> (1993).
- <sup>37</sup>S. G. Claudepierre, I. R. Mann, K. Takahashi, J. F. Fennell, M. K. Hudson, J. B. Blake, J. L. Roeder, J. H. Clemons, H. E. Spence, G. D. Reeves, D. N. Baker, H. O. Funsten, R. H. W. Friedel, M. G. Henderson, C. A. Kletzing, W. S. Kurth, R. J. MacDowall, C. W. Smith, and J. R. Wygant, "Van Allen Probes observation of localized drift resonance between poloidal mode ultra-low frequency waves and 60 keV electrons," *Geophys. Res. Lett.* **40**(17), 4491–4497, <https://doi.org/10.1002/grl.50901> (2013).
- <sup>38</sup>I. R. Mann, E. A. Lee, S. G. Claudepierre, J. F. Fennell, A. Degeling, I. J. Rae, D. N. Baker, G. D. Reeves, H. E. Spence, L. G. Ozeke, R. Rankin, D. K. Milling, A. Kale, R. H. W. Friedel, and F. Honary, "Discovery of the action of a geophysical synchrotron in the Earth's Van Allen radiation belts," *Nat. Commun.* **4**(1), 2795 (2013).
- <sup>39</sup>Q.-G. Zong, X.-Z. Zhou, Y. F. Wang, X. Li, P. Song, D. N. Baker, T. A. Fritz, P. W. Daly, M. Dunlop, and A. Pedersen, "Energetic electron response to ULF waves induced by interplanetary shocks in the outer radiation belt," *J. Geophys. Res.* **114**(A10), A10204, <https://doi.org/10.1029/2009JA014393> (2009).
- <sup>40</sup>M. Yang, X.-Z. Zhou, Q.-G. Zong, L.-F. Zhang, R. Rankin, and Y.-F. Wang, "Traveling ultralow-frequency waves and their influences over low-energy, charged particles," *J. Geophys. Res.* **123**(5), 3848–3858, <https://doi.org/10.1029/2018JA025184> (2018).
- <sup>41</sup>C. L. Tang, X. J. Xie, B. Ni, Z. P. Su, G. D. Reeves, J.-C. Zhang, D. N. Baker, H. E. Spence, H. O. Funsten, J. B. Blake, J. R. Wygant, and G. Y. Dai, "Rapid enhancements of the seed populations in the heart of the Earth's outer radiation belt: A multicase study," *J. Geophys. Res.* **123**(6), 4895–4907, <https://doi.org/10.1029/2017JA025142> (2018).
- <sup>42</sup>C. Cattell, J. R. Wygant, K. Goetz, K. Kersten, P. J. Kellogg, T. von Rosenvinge, S. D. Bale, I. Roth, M. Temerin, M. K. Hudson, R. A. Mewaldt, M. Wiedenbeck, M. Maksimovic, R. Ergun, M. Acuna, and C. T. Russell, "Discovery of very large amplitude whistler-mode waves in Earth's radiation belts," *Geophys. Res. Lett.* **35**(1), L01105, <https://doi.org/10.1029/2007GL032009> (2008).
- <sup>43</sup>R. Goyal, R. P. Sharma, and D. N. Gupta, "Whistler mode localization and turbulence implicating particle acceleration in radiation belts," *Phys. Plasmas* **25**(12), 122903 (2018).

- <sup>44</sup>R. Goyal, R. P. Sharma, and S. Kumar, "Nonlinear effects associated with quasi-electrostatic whistler waves relevant to that in radiation belts," *J. Geophys. Res.* **122**(1), 340–348, <https://doi.org/10.1002/2016JA023274> (2017).
- <sup>45</sup>R. B. Horne, R. M. Thorne, Y. Y. Shprits, N. P. Meredith, S. A. Glauert, A. J. Smith, S. G. Kanekal, D. N. Baker, M. J. Engebretson, J. L. Posch, M. Spasojevic, U. S. Inan, J. S. Pickett, and P. M. E. Decreau, "Wave acceleration of electrons in the Van Allen radiation belts," *Nature* **437**(7056), 227–230 (2005).
- <sup>46</sup>R. P. Lepping, M. H. Acuña, L. F. Burlaga, W. M. Farrell, J. A. Slavin, K. H. Schatten, F. Mariani, N. F. Ness, F. M. Neubauer, Y. C. Whang, J. B. Byrnes, R. S. Kennon, P. V. Panetta, J. Scheifele, and E. M. Worley, "The WIND magnetic field investigation," *Space Sci. Rev.* **71**(1), 207–229 (1995).
- <sup>47</sup>K. W. Ogilvie, D. J. Chornay, R. J. Fritzenreiter, F. Hunsaker, J. Keller, J. Lobell, G. Miller, J. D. Scudder, E. C. Sittler, R. B. Torbert, D. Bodet, G. Needell, A. J. Lazarus, J. T. Steinberg, J. H. Tappan, A. Mavretic, and E. Gergin, "SWE, a comprehensive plasma instrument for the WIND spacecraft," *Space Sci. Rev.* **71**(1), 55–77 (1995).
- <sup>48</sup>D. N. Baker, S. G. Kanekal, V. C. Hoxie, S. Batiste, M. Bolton, X. Li, S. R. Elkington, S. Monk, R. Reukauf, S. Steg, J. Westfall, C. Belting, B. Bolton, D. Braun, B. Cervelli, K. Hubbell, M. Kien, S. Knappmiller, S. Wade, B. Lamprecht, K. Stevens, J. Wallace, A. Yehle, H. E. Spence, and R. Friedel, "The Relativistic Electron-Proton Telescope (REPT) Instrument on Board the Radiation Belt Storm Probes (RBSP) spacecraft: Characterization of Earth's radiation belt high-energy particle populations," *Space Sci. Rev.* **179**(1–4), 337–381 (2012).
- <sup>49</sup>J. B. Blake, P. A. Carranza, S. G. Claudepierre, J. H. Clemons, W. R. Crain, Y. Dotan, J. F. Fennell, F. H. Fuentes, R. M. Galvan, J. S. George, M. G. Henderson, M. Lalic, A. Y. Lin, M. D. Looper, D. J. Mabry, J. E. Mazur, B. McCarthy, C. Q. Nguyen, T. P. O'Brien, M. A. Perez, M. T. Redding, J. L. Roeder, D. J. Salvaggio, G. A. Sorensen, H. E. Spence, S. Yi, and M. P. Zakrzewski, "The Magnetic Electron Ion Spectrometer (MagEIS) Instruments Aboard the Radiation Belt Storm Probes (RBSP) spacecraft," *Space Sci. Rev.* **179**(1), 383–421 (2013).
- <sup>50</sup>N. A. Tsyganenko and M. I. Sitnov, "Modeling the dynamics of the inner magnetosphere during strong geomagnetic storms," *J. Geophys. Res.* **110**(A3), A03208, <https://doi.org/10.1029/2004JA010798> (2005).
- <sup>51</sup>Y. Chen, R. H. W. Friedel, G. D. Reeves, T. G. Onsager, and M. F. Thomsen, "Multisatellite determination of the relativistic electron phase space density at geosynchronous orbit: Methodology and results during geomagnetically quiet times," *J. Geophys. Res.* **110**(A10), A10210, <https://doi.org/10.1029/2004JA010895> (2005).
- <sup>52</sup>B. Ni, Y. Shprits, T. Nagai, R. Thorne, Y. Chen, D. Kondrashov, and H. Kim, "Reanalyses of the radiation belt electron phase space density using nearly equatorial CRRES and polar-orbiting Akebono satellite observations," *J. Geophys. Res.* **114**(A5), A05208, <https://doi.org/10.1029/2008JA013933> (2009).
- <sup>53</sup>C. A. Kletzing, W. S. Kurth, M. Acuna, R. J. MacDowall, R. B. Torbert, T. Averkamp, D. Bodet, S. R. Bounds, M. Chutter, J. Connerney, D. Crawford, J. S. Dolan, R. Dvorsky, G. B. Hospodarsky, J. Howard, V. Jordanova, R. A. Johnson, D. L. Kirchner, B. Mokrzycki, G. Needell, J. Odom, D. Mark, R. Pfaff, J. R. Phillips, C. W. Piker, S. L. Remington, D. Rowland, O. Santolik, R. Schnurr, D. Sheppard, C. W. Smith, R. M. Thorne, and J. Tyler, "The Electric and Magnetic Field Instrument Suite and Integrated Science (EMFISIS) on RBSP," *Space Sci. Rev.* **179**(1), 127–181 (2013).
- <sup>54</sup>J.-H. Shue, J. K. Chao, H. C. Fu, C. T. Russell, P. Song, K. K. Khurana, and H. J. Singer, "A new functional form to study the solar wind control of the magnetopause size and shape," *J. Geophys. Res.* **102**(A5), 9497–9511, <https://doi.org/10.1029/97JA00196> (1997).
- <sup>55</sup>J. M. Albert, R. S. Selesnick, S. K. Morley, M. G. Henderson, and A. C. Kellerman, "Calculation of last closed drift shells for the 2013 GEM Radiation Belt Challenge events," *J. Geophys. Res.* **123**(11), 9597–9611, <https://doi.org/10.1029/2018JA025991> (2018).